LIMNOLOGY and OCEANOGRAPHY

ASLO

Limnol. Oceanogr. 62, 2017, 1984–2003

doi: 10.1002/lno.10547

Thaumarchaeal ecotype distributions across the equatorial Pacific Ocean and their potential roles in nitrification and sinking flux attenuation

Alyson E. Santoro [1,a]* Mak A. Saito,[2] Tyler J. Goepfert,[2,b] Carl H. Lamborg,[3] Chris L. Dupont,[4] Giacomo R. DiTullio[5]

[1]Horn Point Laboratory, University of Maryland Center for Environmental Science, Cambridge, Maryland
[2]Department of Marine Chemistry and Geochemistry, Woods Hole Oceanographic Institution, Woods Hole, Massachusetts
[3]Department of Ocean Sciences, University of California, Santa Cruz, California
[4]J. Craig Venter Institute, San Diego, California
[5]Hollings Marine Laboratory, College of Charleston, Charleston, South Carolina

Abstract

Thaumarchaea are among the most abundant microbial groups in the ocean, but controls on their abundance and the distribution and metabolic potential of different subpopulations are poorly constrained. Here, two ecotypes of ammonia-oxidizing thaumarchaea were quantified using ammonia monooxygenase (*amoA*) genes across the equatorial Pacific Ocean. The shallow, or water column "A" (WCA), ecotype was the most abundant ecotype at the depths of maximum nitrification rates, and its abundance correlated with other biogeochemical indicators of remineralization such as NO_3 : Si and total Hg. Metagenomes contained thaumarchaeal genes encoding for the catalytic subunit of the urease enzyme (*ureC*) at all depths, suggesting that members of both WCA and the deep, water column "B" (WCB) ecotypes may contain *ureC*. Coupled urea hydrolysis-ammonia oxidation rates were similar to ammonia oxidation rates alone, suggesting that urea could be an important source of ammonia for mesopelagic ammonia oxidizers. Potential inducement of metal limitation of both ammonia oxidation and urea hydrolysis was demonstrated via additions of a strong metal chelator. The water column inventory of WCA was correlated with the depth-integrated abundance of WCB, with both likely controlled by the flux of sinking particulate organic matter, providing strong evidence of vertical connectivity between the ecotypes. Further, depth-integrated *amoA* gene abundance and nitrification rates were correlated with particulate organic nitrogen flux measured by contemporaneously deployed sediment traps. Together, the results refine our understanding of the controls on thaumarchaeal distributions in the ocean, and provide new insights on the relationship between material flux and microbial communities in the mesopelagic.

Microbial diversity in the ocean is vast, even within co-existing, closely related groups of microorganisms. Within this diverse assemblage, the distribution of specific microbial ecotypes—ecologically differentiated but phylogenetically similar populations (Cohan 2001)—should be shaped by the physicochemical features of the surrounding environment. In the ocean, the ecotype framework has been applied to explain diversity patterns in some of the most abundant bacterial groups (reviewed in Cordero and Polz 2014). For example, ecotypes of the cyanobacterium *Prochlorococcus* appear closely tied to light physiology (Moore et al. 1998) and vary predictably with temperature and light both temporally (Malmstrom et al. 2010) and across basin-scale gradients (Johnson et al. 2006; Zinser et al. 2007). Similarly, ecotypes of abundant heterotrophic bacterial clades vary predictably with temperature, depth, and season such as SAR11 in the Sargasso Sea (Carlson et al. 2009) and SAR86 in the surface ocean (Dupont et al. 2012). Marine ecosystem models that

*Correspondence: asantoro@ucsb.edu

[a]Present address: Department of Ecology, Evolution, and Marine Biology, University of California, Santa Barbara, California

[b]Division of Marine Geosystems, Helmholtz Center for Ocean Research, Kiel, Germany

Additional Supporting Information may be found in the online version of this article.

include the physiological adaptations of these ecotypes are successful at recreating microbial biogeography (Follows et al. 2007). While efforts to date have focused primarily on taxa in the surface and upper mesopelagic ocean, similar gradients in temperature and material flux exist throughout the mesopelagic. Yet, there are remarkably few quantitative, taxon-specific studies of planktonic microbes in the mesopelagic.

Thaumarchaeota are one of the most abundant microbial groups in the mesopelagic and deep oceans (Karner et al. 2001) and offer an attractive system for quantitative mapping of ecotypes across basin-scale physicochemical gradients. Thaumarchaea have been directly linked to nitrogen remineralization in the upper ocean through their role in the oxidation of ammonia (NH_3) to nitrite (NO_2^-), the first step of nitrification (Konneke et al. 2005; Wuchter et al. 2006). In the marine water column, ammonia-oxidizing thaumarchaea far exceed their bacterial counterparts, particularly in the open ocean (Santoro et al. 2010). The hypothesized basis for this dominance is their high substrate affinity for NH_3/NH_4^+ (Martens-Habbena et al. 2009), making these organisms ideally suited to the extremely low NH_3/NH_4^+ flux in the open ocean (Gruber 2008). Early studies of thaumarchaeal ammonia monooxygenase subunit A (*amoA*) gene sequences from the ocean recovered two distinct clades of pelagic ammonia-oxidizing thaumarchaea (Francis et al. 2005), termed water column "A" (WCA) and water column "B" (WCB), that have been suggested to represent "shallow" and "deep" adapted ecotypes (Hallam et al. 2006; Mincer et al. 2007; Beman et al. 2008) within the marine thaumarchaea (Pester et al. 2011). Subsequent studies supported this hypothesis, with depth being a significant factor controlling ammonia-oxidizing archaeal community composition (Biller et al. 2012; Sintes et al. 2015) and observations of increasing WCB-like *amoA* gene abundance with depth (Santoro et al. 2010; Smith et al. 2014, 2015).

Despite an emerging understanding of the biogeography of thaumarchaea, the physiological basis for the WCA-WCB clade division has not been definitively identified. Depth in the ocean corresponds with gradients in nearly every physicochemical parameter including temperature, light, and organic matter flux. Only one cultivated representative of the shallow WCA clade has been described, *Candidatus* "Nitrosopelagicus brevis" (Santoro and Casciotti 2011; Santoro et al. 2015) and as-yet, there are no cultivated representatives of the WCB clade. Thus, exploring the physiological basis of the ecotype division is not yet possible with cultivated organisms. Though there are significant differences in gene content between pelagic and benthic thaumarchaea (Swan et al. 2014; Santoro et al. 2015), cultivation-independent single cell and metagenomic studies have suggested limited identifiable gene content differences between the shallow and deep pelagic thaumarchaea (Luo et al. 2014). One hypothesized difference between the two ecotypes is tolerance to sunlight, as DNA photolyase was detected exclusively in the epipelagic clade (Luo et al. 2014). This protein, however, is expressed in the dark (Santoro et al. 2015), thus its role in adaptation to light stress is uncertain. Other hypotheses put forth to explain the ecotype distributions include substrate affinity (Sintes et al. 2013; Smith et al. 2015) or the ability to use organic substrates other than reduced nitrogen as sources of energy and reducing equivalents (Qin et al. 2014). For example, at least some thaumarchaea in the ocean appear to be able to use urea (Alonso-Saez et al. 2012; Qin et al. 2014; Swan et al. 2014). Differential requirements for micronutrients, such as copper (Amin et al. 2013), may also explain niche differentiation between the two ecotypes, but as yet are unexplored.

As thaumarchaea are a dominant taxon in the dark ocean, quantitative mapping of thaumarchaea may help inform some long-standing questions about energy supply to the deep ocean, and the relationship between material export from the surface and its impact on microbial communities below (Cho and Azam 1988). Studies in the Pacific have found a general correspondence between latitudinal patterns in particulate organic matter (POM) flux and microbial abundance in the meso- and bathyplelagic (Nagata et al. 2000; Yokokawa et al. 2013), while no relationship was found across spatial gradients in POM flux in the Arabian Sea (Hansell and Ducklow 2003). The same study, however, found a relationship between annual POM flux and bathypelagic microbial abundance, leading to the conclusion that bathypelagic microbial abundance integrates across a long-term average of material flux. These previous studies used cell count methods that cannot resolve individual microbial groups. With the ability to quantify genes at a resolution previously possible only with cell counts, relationships between individual microbial taxa and organic matter export can now be explored.

Motivated by a desire to understand both the distribution of thaumarchaeal ecotypes and the relationships between material export, nitrogen remineralization, and the abundance of thaumarchaea in the mesopelagic, here, we examine the distribution of thaumarchaea across a transect in the equatorial Pacific, a region of previous intensive investigation of carbon export (Murray et al. 1995). Spatial mapping of the two thaumarchaeal ecotypes is compared to a suite of physicochemical parameters to identify physical and biological factors that could contribute to the distribution of each ecotype across multiple biogeographic provinces. Rate experiments using $^{15}NH_4^+$ and ^{15}N-urea were conducted at a subset of sites to characterize the biogeochemical environment with respect to nitrogen remineralization. These experiments included treatments to identify the potential for trace metal limitation of urea hydrolysis and nitrification, which rely on metalloenzymes (Morel and Price 2003; Walker et al. 2010). The results are compared to contemporaneous measurements of particulate organic nitrogen (PON) flux

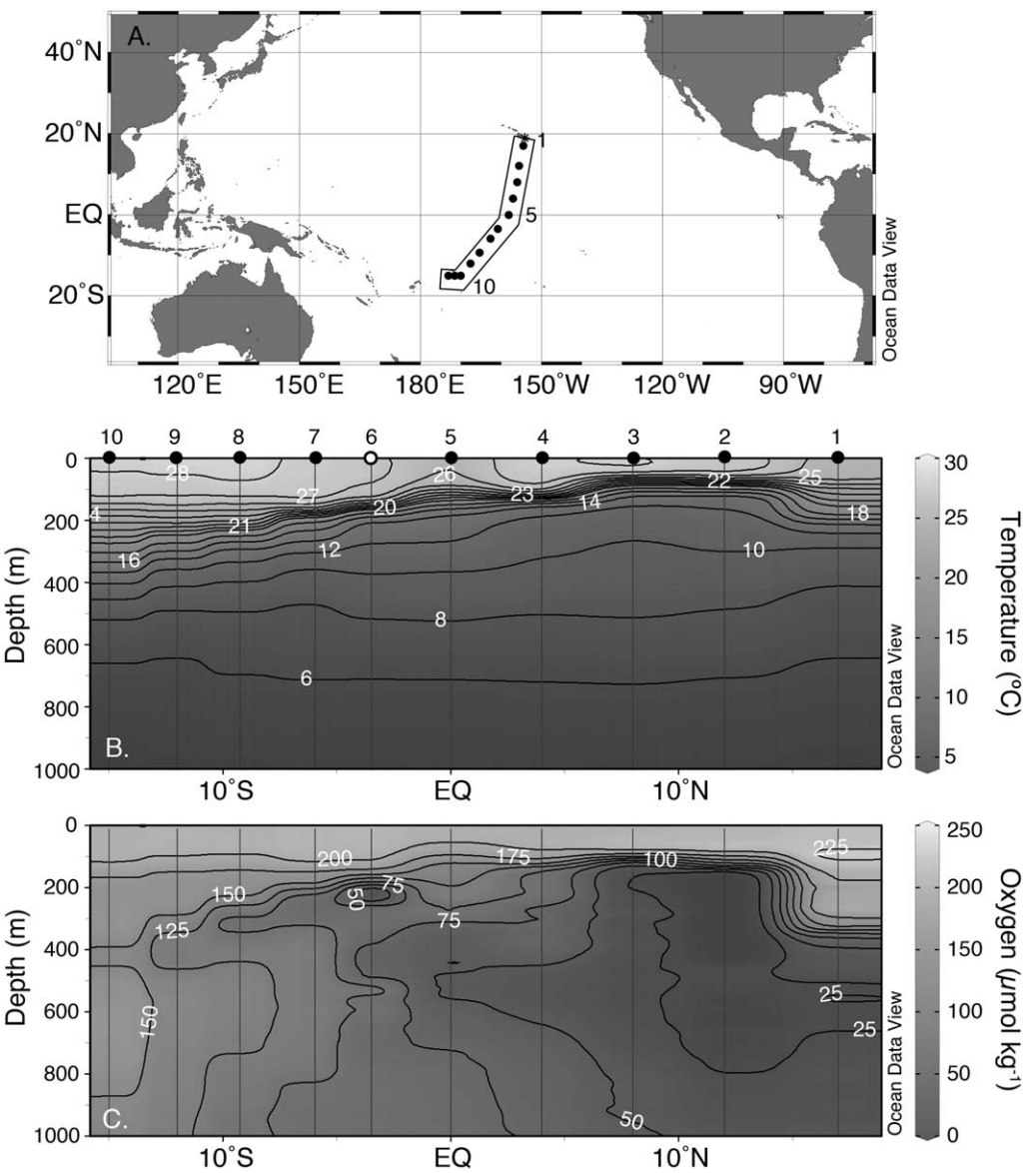

Fig. 1. (**A**) Location of the METZYME cruise across the equatorial Pacific. (**B**) Temperature and (**C**) oxygen concentration across the cruise track. Temperature and oxygen data are reported as 1 m-binned averages from the CTD sensors. Station locations are indicated as black circles with station numbers above. Open circle denotes a station where only physicochemical samples (i.e., no molecular samples) were collected (station 6). Data were contoured using weighted-average gridding in Ocean Data View v4.7.3.

using sediment traps. This study is unique in that it examines the distribution of thaumarchaea over a rarely examined spatial and depth scale, ties these measurements directly to particulate flux measurements, and examines them against a rich dataset of accompanying environmental parameters.

Materials and methods

Cruise track and sample collection

Samples were collected 01 October 2011–25 October 2011 during the METZYME cruise (KM1128) aboard the R/V *Kilo Moana* (Lamborg et al. 2014; Saito et al. 2014). The cruise track was an ~ 4500 km transect from Hawai'i, across the equatorial upwelling region, and west to the islands of Samoa (Fig. 1A). Eleven oceanographic stations were sampled for molecular characterization of thaumarchaea. A subset of three stations (stations 1, 3, and 5) was chosen for additional geochemical characterization using stable isotope labeling experiments; two of these (stations 3 and 5) were chosen for metagenomic sequencing at select depths (see below).

Water samples were collected at discrete depths using either a standard 24-bottle rosette sampler equipped with an SBE9plus conductivity–temperature–depth (CTD) sensor package (SeaBird Electronics, Bellevue, Washington) or a 12-bottle

trace metal clean rosette equipped with an SBE19 CTD. Nutrient samples were collected from the trace metal clean rosette at 12 depths between 0 m and 1000 m and stored frozen until analysis. Samples for nucleic acid extraction were collected from the rosette in 2–4 L polycarbonate bottles. With one exception, samples were collected from at least ten depths between 40 m and 1000 m, with additional sampling to 3000 m at stations 5, 9, and 11. Fewer samples were collected at station 4 due to loss of the ship's CTD rosette sampler; a reconstituted equipment package was used in subsequent stations lacking only a PAR sensor. Cells were harvested by pressure filtration onto 25 mm diameter, 0.2 μm pore-size polyethersulfone membrane filters (Supor-200, Pall Corporation, Port Washington, New York) housed in polypropylene filter holders (Whatman SwinLok, GE Healthcare, Pittsburgh, Pennsylvania) using a peristaltic pump and silicone tubing. Pump tubing was acid washed with 10% hydrochloric acid and flushed with ultrapure water between each sample. For DNA extraction and analysis, 1–4 L sample volumes were filtered depending on the biomass present at each station and depth, and the filters were flash frozen in liquid nitrogen in 2 mL gasketed bead beating tubes (Fisher Scientific).

Samples for metagenomic sequencing were collected from the 0.2–3.0 μm plankton size fraction using an in situ pumping system (McLane Research Laboratories, East Falmouth, Massachusetts) and captured on 142 mm, 0.2 μm pore size Supor-200 filters (Pall) as described previously (Saito et al. 2014). Filters were sectioned immediately after pump recovery and approximately one quarter of the filter was stored at −80°C for later DNA extraction and sequencing (see below). Metagenomic samples were collected from station 3 at five depths: 150 m, 250 m, 300 m, 550 m, 800 m, and from station 5 at 50 m.

Nutrient analyses

Dissolved nitrite (NO_2^-), nitrite+nitrate ($NO_2^- + NO_3^-$), ammonium (NH_4^+), ortho-phosphate, and silicate concentrations were determined from thawed seawater samples using standard colorimetric methods at the Oregon State University College of Earth, Ocean and Atmospheric Sciences nutrient laboratory. Nutrient, mercury (Hg) speciation, and high-performance liquid chromatography (HPLC) pigment data from the cruise have been reported previously (Saito et al. 2014; Munson et al. 2015) and were used in the present data analysis. At the three stations where nitrification rates were measured (see below), low level ammonium concentrations [NH_4^+] were quantified at 7–10 depths in the upper 200 m at sea with the *o*-phthaldialdehyde fluorescence method (Holmes et al. 1999; Taylor et al. 2007) using duplicate 50 mL sample volumes with a detection limit of 31 nM. Dissolved urea concentration was determined colorimetrically using the diacetyl monoxime method (Price and Harrison 1987) with previously frozen samples from the initial timepoints of the ^{15}N-urea addition experiments (see below) using 10 mL sample volumes with a detection limit of 100 nM.

Nitrification rate measurements

Rate measurements were conducted using stable isotope tracer additions (^{15}N) at stations 1, 3, and 5 at four depths in the upper water column, targeting the base of the subsurface chlorophyll maximum as the shallowest depth and at approximately 75 m intervals below. Water for incubations at station 1 was obtained from the ship's rosette; water for stations 3 and 5 was obtained from the trace metal clean rosette due to the aforementioned equipment loss. For each depth, three 500 mL bottle incubations were conducted: two ammonia oxidation rate bottles (with $^{15}NH_4^+$ added) and one no-addition control bottle. Water for the experimental bottles was collected directly from the rosette into 500 mL acid-cleaned polycarbonate bottles. Each bottle was spiked with 100 μL of 1 mmol L^{-1} ^{15}N-labeled substrate ($^{15}NH_4^+$, 99.5 atom percent ^{15}N; equivalent to a final label concentration of 200 nmol L^{-1} ^{15}N, Cambridge Isotope Laboratories). Bottles for the surface chlorophyll maximum depth (approximately 1% surface irradiance) incubations were incubated in an on-deck circulating seawater incubator in neutral density-screened bags calibrated to approximate the in situ light field at each depth using a photosynthetically active radiation sensor (Biospherical Instruments QSL-2200). Waters from below the euphotic zone were incubated at approximately in situ temperatures in the dark in commercial refrigeration units.

Replicate 50 mL samples were removed from each bottle at time points of 0 h, 8 h, 16 h, and 24 h, 0.2 μm syringe-filtered, and frozen. Samples were prepared for $\delta^{15}N_{NOx}$ determination from 10 nmol or 20 nmol of analyte using the denitrifier method (Sigman et al. 2001; Mcilvin and Casciotti 2011) at the University of Maryland Center for Environmental Science. Isotopic analysis of the resulting headspace N_2O used a ThermoFinnigan Delta^{PLUS} V isotope ratio mass spectrometer interfaced with a ThermoFinnigan GasBench II-PreCon trace gas analysis system at the University of California, Davis Stable Isotope Facility. $\delta^{15}N_{NOx}$ values were calibrated against NO_3^- isotope reference materials USGS32, USGS34, and USGS35, analyzed in parallel.

Nitrification rates were calculated using the model described previously (Santoro et al. 2013). Model coefficients F_{in} (the rate of NO_x^- production, with units μmol L^{-1} h^{-1}) and k (the rate constant for NO_2^- or NO_x^- assimilation, with units h^{-1}) were calculated using a non-linear least squares curve fitting routine, implemented in MATLAB R2011b with the Optimization Toolbox. The fractionation factor for NO_x assimilation (α) was taken to be 1.005. Standard error in the fit coefficients was calculated by approximating the covariance matrix, and using the square root of the diagonal to calculate the standard error. Isotope dilution of the tracer (Glibert et al. 1982) and rate stimulation by tracer addition (Horak et al. 2013) can lead to under or over estimation of

the calculated rates, respectively. No corrections for either process have been applied to the rates calculated here.

Urea hydrolysis and trace metal limitation experiments

A set of additional incubations were conducted at station 3 to determine rates of nitrification and urea hydrolysis coupled to nitrification, and to assess the effect of induced metal limitation on these processes via the addition of the metal-chelating ligand TETA. Here we use TETA to describe the molecule 1,4,8,11-tetraazacyclotetradecane-1,4,8,11-tetraacetic acid hydrochloride hydrate, abbreviated TETA by Martell and Smith (1977). However, caution is advised not to confuse this molecule with another Cu chelator named TETA, triethylenetetramine. The TETA molecule utilized here has a strong affinity for Cu and Co; thermodynamic stability constants for TETA show an affinity for metals in the order Cu, Co, Ni, Zn, Fe(III), and Fe(II) (listed in order of decreasing stability constants; 0.1 ionic strength and 25°C; Martell and Smith 1977). Water for these experiments was collected at 150 m and 300 m depths using the trace metal clean rosette described above. For each treatment, triplicate trace metal clean 250 mL polycarbonate bottles were triple rinsed and filled within a temporary clean room on the ship. The treatments were: (1) 100 nM natural abundance NH_4^+, (2) 50 nM natural abundance urea, (3) 100 nM $^{15}NH_4^+$, (4) 50 nM ^{15}N-urea, and (5) ^{15}N urea plus 0.1 μM TETA. Experiments were harvested after 32 h. As only two time points were available for urea-based nitrification rate determination, the linear equations of Dugdale and Goering (1967) were used to calculate the rate of $^{15}NO_x$ production over time.

Nucleic acid extraction

Nucleic acids (DNA) were extracted as described previously (Santoro et al. 2010), with slight modifications. Briefly, cells on the filters were lysed directly in the bead beating tubes with sucrose-ethylene diamine tetraacetic acid (EDTA) lysis buffer (0.75 M sucrose, 20 mM EDTA, 400 mM NaCl, 50 mM Tris) and 1% sodium dodecyl sulfate (SDS). Prior to mechanical lysis, filter samples were subject to three freeze-thaw cycles of 5 min in liquid nitrogen and 5 min in a 65°C water bath. Tubes were then agitated in a FastPrep bead beating machine (MP Biomedicals) for 1.5 min at speed 5.5, and proteinase K (Invitrogen) was added to a final concentration of 0.5 mg mL^{-1}. Filters were incubated at 55°C for approximately 4 h and the resulting lysates were purified with the DNeasy kit (Qiagen) using a slightly modified protocol (Santoro et al. 2010). The purified nucleic acids were eluted in 200 μL of DNase, RNase-free water (Gibco), and quantified using a fluorometer (Qubit and Quanti-T BR reagent, Invitrogen Molecular Probes).

DNA for metagenomic library construction and sequencing was extracted as previously described (Rusch et al. 2007). Briefly, TE buffer (pH 8) containing 50 mM ethylene glycol tetraacetic acid (EGTA) and 50 mM EDTA was added until filter pieces were barely covered. Lysozyme was added to a final concentration of 2.5 mg mL^{-1}, and the tubes were incubated at 37°C for 1 h. Proteinase K was added to a final concentration of 200 μg mL^{-1}, and the samples were subjected to two cycles of rapid freeze-thaw. SDS (final concentration of 1%) and an additional 200 μg mL^{-1} of proteinase K were added, and samples were incubated at 55°C for 2 h followed by three aqueous phenol extractions and one phenol/chloroform extraction. The supernatant was then precipitated with two volumes of 100% ethanol, and the DNA pellet was washed with 70% ethanol. Finally, DNA was treated with cetyl trimethylammonium bromide (CTAB) to remove enzyme inhibitors.

Quantitative PCR (qPCR)

All qPCR assays were conducted using group-specific assays for the thaumarchaeal *amoA* gene for WCA and WCB ecotypes (Mosier and Francis 2011) with TaqMan Environmental Mastermix (Life Technologies) chemistry on a CFX96 qPCR machine (Bio-Rad, Hercules, California). Detection limits for TaqMan assays were 1 copy mL^{-1} or better. All samples were run in triplicate against a standard curve spanning approximately 10^1-10^5 templates, run in duplicate. Plasmids containing cloned inserts of the target gene (TOPO pCR4 vector, Invitrogen or pGem vector, Promega) were used as standards. Standards were linearized with the restriction enzyme NotI (New England Biolabs), purified (DNeasy, Qiagen), quantified by fluorometry (Quanti-T HS reagent, Invitrogen), and stored at −80°C. Fresh standard dilutions were made from frozen stocks for each day of analysis. qPCR was carried out using the following thermal profile: 95°C for 10 min, followed by 40 cycles of 95°C for 30 s and 55°C for 30 s. A minimum of three negative control qPCR reactions to which no DNA template was added were run with every assay. Efficiency was calculated relative to a theoretical standard curve slope of 3.32. All qPCR runs were setup using an epMotion 5070 automated liquid handling system (Eppendorf) to minimize between-run variability. A total of 148 samples were analyzed for each ecotype assay.

Metagenomic sequencing and bioinformatic analysis

Metagenomic sequence data were produced by the United States Department of Energy Joint Genome Institute (JGI; http://www.jgi.doe.gov/), in collaboration with the user community, following standard JGI protocols for library generation, sequencing, and assembly on the Illumina HiSeq 2000 or 2500 sequencing platforms. Thaumarchaeal *amoA*, urease gamma subunit (*ureC*), and ammonium transporter (*amtB1*) genes were identified through blastn searches using reference genes from all full genome-sequenced marine thaumarchaea and a thaumarchaeal *ureC* gene obtained from a urea-hydrolyzing enrichment culture (P. Carini, Santoro and Dupont, unpubl.) against the assembled metagenomic data using a 70% nucleotide identity threshold and 50% coverage requirement. Thaumarchaeal 16S rRNA sequences were identified using a 90% nucleotide identity threshold to genome-

Table 1. Summary of hydrographic parameters on the METZYME cruise, October 2011. Depth integrated nitrification rates are calculated from the base of the euphotic zone and 300 m. Chl *a* concentrations reported are the sum of Chl *a* and divinyl Chl *a*.

Station	Lat.	Long.	SST (°C)	ML depth (m)	ML $[NO_3^-]$ (μM)	Surface [Chl *a*] (ng L^{-1})	Depth of DCM - CTD (m)	Depth of DCM - HPLC (m)	[Chl *a*] at DCM (ng L^{-1})	Depth of O_2 min (m)	Min $[O_2]$ (μmol kg^{-1})	PON flux at 60 m ± SD (mmol m^{-2} d^{-1})*	Depth-integrated nitrification rate (mmol m^{-2} d^{-1})
1	17.0	−154.4	25.7	48	BDL	28	124	87	205	499	18	0.61 ± 0.28	0.39
2	12.0	−155.5	27.3	53	BDL	34	ND	100	315	142	1	ND	ND
3	8.0	−156.0	28.3	37	0.31	79	ND	80	340	146	12	1.09 ± 0.35	0.92
4	4.0	−157.1	28.1	101	1.77	187	21	200	249	473	38	ND	ND
5	0.0	−157.1	25.9	57	6.10	277	43	40	448	511	37	1.55 ± 0.33	2.17
6	−3.5	−160.8	27.3	104	5.10	220	72	60	391	216	24	ND	ND
7	−6.0	−162.6	27.8	136	4.32	162	84	85	315	267	76	ND	ND
8	−9.25	−165.4	28.5	61	1.46	110	69	60	396	327	89	ND	ND
9	−12.0	−167.6	28.9	23	0.67	133	57	60	415	400	111	ND	ND
10	−15.0	−170.0	28.2	90	0.17	44	136	135	475	443	134	ND	ND
11	−15.0	−171.5	28.2	57	0.91	ND	137	ND	ND	438	137	ND	ND
12	−15.0	−173.1	28.4	71	0.12	80	114	125	510	402	114	ND	ND

SST, sea surface temperature; ML, mixed layer; defined as 0.5°C temperature deviation from SST; DCM, deep Chl *a* maximum; BDL, below detection limit; ND, not determined.
* From Munson et al. (2015).

sequenced marine thaumarchaea. Coverage information of the raw reads to the assembled contigs was taken directly from the mapping to assemblies generated by JGI. Nucleotide sequence alignments were performed using MAFFT's local pairwise alignment algorithm (L-INS-i; v7.245, Katoh and Standley 2013) with default settings and manually refined based on the translated sequences in AliView (Larsson 2014). Phylogenetic trees were constructed using FastTree (Price et al. 2009) using the GTR + CAT model for nucleotide trees and the WAG + CAT model for the AmtB amino acid tree.

Statistical analyses

All curve fitting and statistical analyses were implemented in MATLAB R2011b (MathWorks, v.7.13) using the Statistics and Curve Fitting Toolboxes. Pairwise correlation analyses used non-parametric Spearman correlations and partial Spearman correlations on untransformed data using the functions "corr" and "partialcorr." Stepwise regression models ("stepwisefit") were evaluated on de-meaned data normalized to a standard deviation of 1. Non-parametric fitting using multiple methods (first-order polynomial, smoothing spline, and local interpolation) was used to investigate the relationship between thaumarchaeal community structure (as %WCB) and physicochemical variables. To investigate relationships through the vertical extent of the water column, biological variables (qPCR and pigment data) were depth-integrated between 10 m and 1000 m using trapezoidal integration and analyzed using non-parametric correlation analysis as above.

Data deposition

All nutrient, qPCR, and nitrification rate data have been archived with the United States National Science Foundation's Biological and Chemical Oceanography Data Management Office (BCO-DMO; bco-dmo.org) in association with the "MetZyme" project. Metagenomic data (both raw data and assemblies) are available in JGI's Integrated Microbial Genomes database (img.jgi.doe.gov) under JGI Project ID numbers 1024961, 1024964, 1024967, 1024970, 1024973, and 1024976. Sequence alignments have been archived with BCO-DMO, also in association with the MetZyme project.

Results

General hydrographic parameters

Sampling extended from the oligotrophic waters of the North Pacific Subtropical Gyre, off the Hawaiian Islands (station 1), across the Equator (station 5) along 157°W, then west to Western Samoa (station 12; Fig. 1A; Table 1). Surface temperature along this transect varied from 25.7°C (station 1) to 28.9°C (station 9) (Table 1; Fig. 1B). At station 5, the equatorial upwelling was evident in lower SST than adjacent stations, concave isothermals, and elevated surface $[NO_3^-]$ of 6.1 μM (Table 1). Chlorophyll *a* (Chl *a*) concentration was

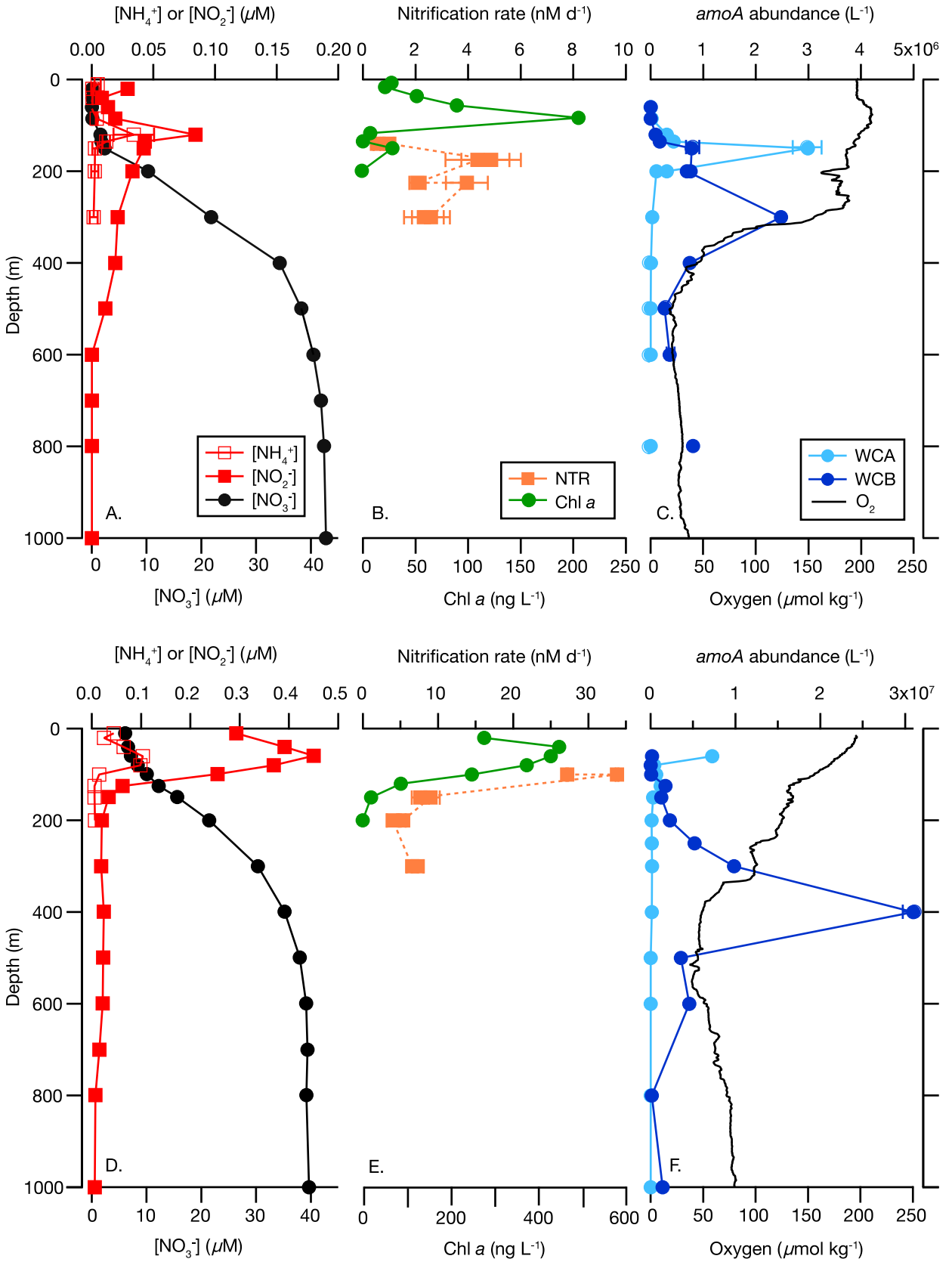

Fig. 2. Representative depth profiles from station 1 (17° N, top row) and station 5 (Equator, bottom row) (**A**, **D**). $[NH_4^+]$ (open squares), $[NO_2^-]$ (filled squares), $[NO_3^-]$ (filled circles). Error bars for $[NH_4^+]$ measurements represent standard error of triplicate measuremetns and in most cases are smaller than the symbol (**B**, **E**). Nitrification rates (NTR) determined using $^{15}NH_4Cl$ (filled squares) and Chl *a* determined using high performance liquid chromatography (filled circles). Error bars for NTR indicate standard error in the model fit, and in most cases are smaller than the symbol; (**C**, **F**). Abundance of archaeal *amoA* genes determined using qPCR for the water column "A" (WCA) and water column "B" (WCB) ecotypes, and dissolved oxygen. Points are the mean of triplicate qPCR analyses; error bars indicade standard deviation from the mean and in most cases are smaller than the symbol. Note that scaling changes on most horizontal axes between stations.

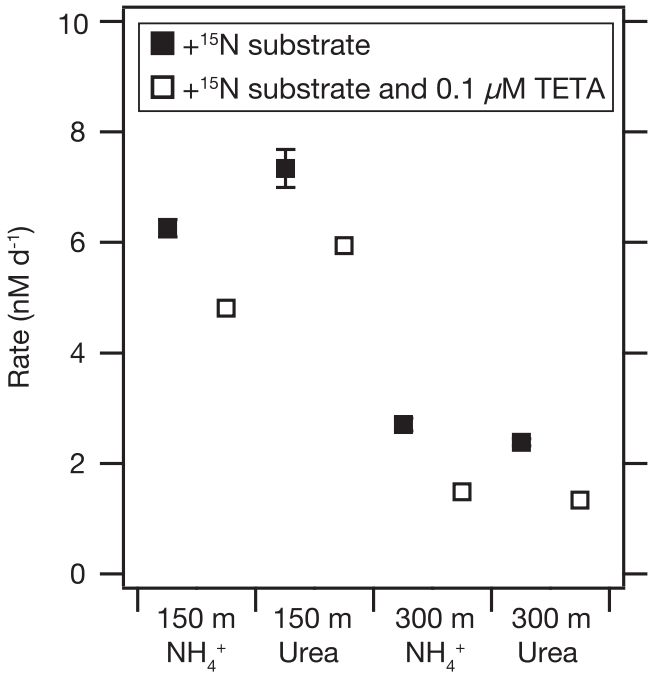

Fig. 3. Rates of nitrification and coupled urea hydrolysis-nitrification at station 3 determined under trace-metal clean conditions using ^{15}N tracers with and without the divalent metal chelator TETA. In all cases, rates in the TETA addition bottles are significantly lower (Student's *t*-test, $p < 0.02$ for all pairwise comparisons). Values are the means of triplicate experimental bottles for each treatment. Error bars indicate one standard error and in most cases are smaller than the symbol.

also high at station 5, both at the surface (277 ng L^{-1}; Table 1) and in the deep Chl *a* maximum (DCM, 448 ng L^{-1}). The highest subsurface Chl *a* concentrations were observed at the western edge of the cruise track at stations 10 and 12 (475–510 ng L^{-1}). The cruise track intersected the western extent of the Eastern Tropical North Pacific oxygen deficient zone at stations 2 and 3, with low mesopelagic oxygen concentrations approaching the detection limit of the standard CTD oxygen sensor (~ 1 μM) (Table 1). [NH_4^+] and [NO_2^-] profiles demonstrated characteristic maxima just below the DCM (Fig. 2). [NH_4^+] in the NH_4^+ maximum ranged from 34 nM at station 1 (Fig. 2A) in the North Pacific Subtropical Gyre to 103 nM at station 5 at the Equator (Fig. 2D). The subsurface NO_2^- maximum (the primary nitrite maximum) ranged from very low values in the gyre (station 1) and off Samoa (0.05–0.08 μM; stations 10–12) to 2.15 μM at station 7 (Fig. 2A,D; Table 1). Urea concentrations at station 3, the only station analyzed, were 38 nM at 150 m and below the detection limit at 300 m.

Nitrification rate distributions

Nitrification rates in the oligotrophic gyre at station 1 ranged from 0.8 nM d^{-1} below the chlorophyll maximum (140 m; Fig. 2B) to 4.6 nM d^{-1} at 175 m. At station 3, nitrification rates varied little across the 4 depths sampled, ranging from 3.5 nM d^{-1} at 300 m to 4.4 nM d^{-1} at 150 m and 225 m (Supporting Information Table S1). Relatively high rates of nitrification were measured at the Equator, station 5 (Fig. 2E), reaching 30.5 nM d^{-1} within the subsurface NO_2^- maximum and decreasing to 4.6 nM d^{-1} at 200 m. No changes in $\delta^{15}N_{NOx}$ were detected in the no-addition controls at any station/depth (data not shown).

Additional experiments were conducted at station 3 (150 m and 300 m depths) to determine rates of coupled urea hydrolysis-nitrification, and the impact of free metal chelation on the rates of those processes (Fig. 3). At 150 m, rates of coupled urea hydrolysis-nitrification were slightly, but significantly, higher than nitrification alone (Fig. 3A; 7.3 ± 0.3 nM d^{-1} vs. 6.3 ± 0.2 nM d^{-1}; *t*-test, $p = 0.05$). At 300 m, rates of the two processes were not significantly different (2.4 ± 0.1 nM d^{-1} vs. 2.7 ± 0.1 nM d^{-1}; $p = 0.07$). Addition of the metal chelator TETA significantly decreased both nitrification and coupled urea hydrolysis-nitrification at both depths (Fig. 3). TETA addition to a final concentration of 0.1 μM reduced nitrification rates 23% to 4.8 ± 0.02 nM d^{-1} at 150 m. Coupled urea hydrolysis-nitrification was similarly affected, decreasing 19% to 5.9 ± 0.3 nM d^{-1}. Rates at 300 m were more affected by TETA addition, with nitrification decreasing 45% to 1.5 ± 0.1 nM d^{-1} and coupled urea hydrolysis-nitrification decreasing 44% to 1.3 ± 0.1 nM d^{-1}.

Thaumarchaeal ecotype distributions

The WCA clade of *amoA*-containing archaea is thought to be adapted to the epipelagic, while the WCB clade is thought to be adapted to the mesopelagic. The general shape of depth profiles of WCA *amoA* genes was as follows: low to undetectable in the mixed layer, maximal near the top of the nitracline, becoming very low ($< 10^5$ genes L^{-1}) again below 200 m (Fig. 2C,F). Across the cruise track (Fig. 4A), abundances of WCA *amoA* genes were lowest at station 1, ranging from below detection limits in surface waters and below 500 m to approximately 3.0×10^6 genes L^{-1} at the top of nitracline. Abundance of WCA *amoA* genes was relatively high at station 5, reaching 7.3×10^6 genes L^{-1} at 60 m, but reached the maximum abundance at station 10, 175 m depth (1.8×10^7 genes L^{-1}) within a mesopelagic feature containing high abundances of both thaumarchaeal clades at stations 9–12 (Fig. 4A,B). WCA *amoA* gene abundance was correlated ($p < 0.05$) with over 20 hydrographic parameters (Table 2), exhibiting the strongest correlations with NO_3 : Si ($r = 0.58$), the pelagophyte pigment 19′-butanoyloxyfucoxanthin ($r = 0.41$), and a negative correlation with the cyanobacterial pigment zeaxanthin ($r = -0.52$). WCA *amoA* abundance was not correlated with nitrification rate ($p = 0.12$), but was inversely correlated with [NH_4^+] ($r = -0.23$, $p = 0.02$). Stepwise regression modeling was further applied to establish predictive relationships between measured physicochemical and biological parameters. Of the

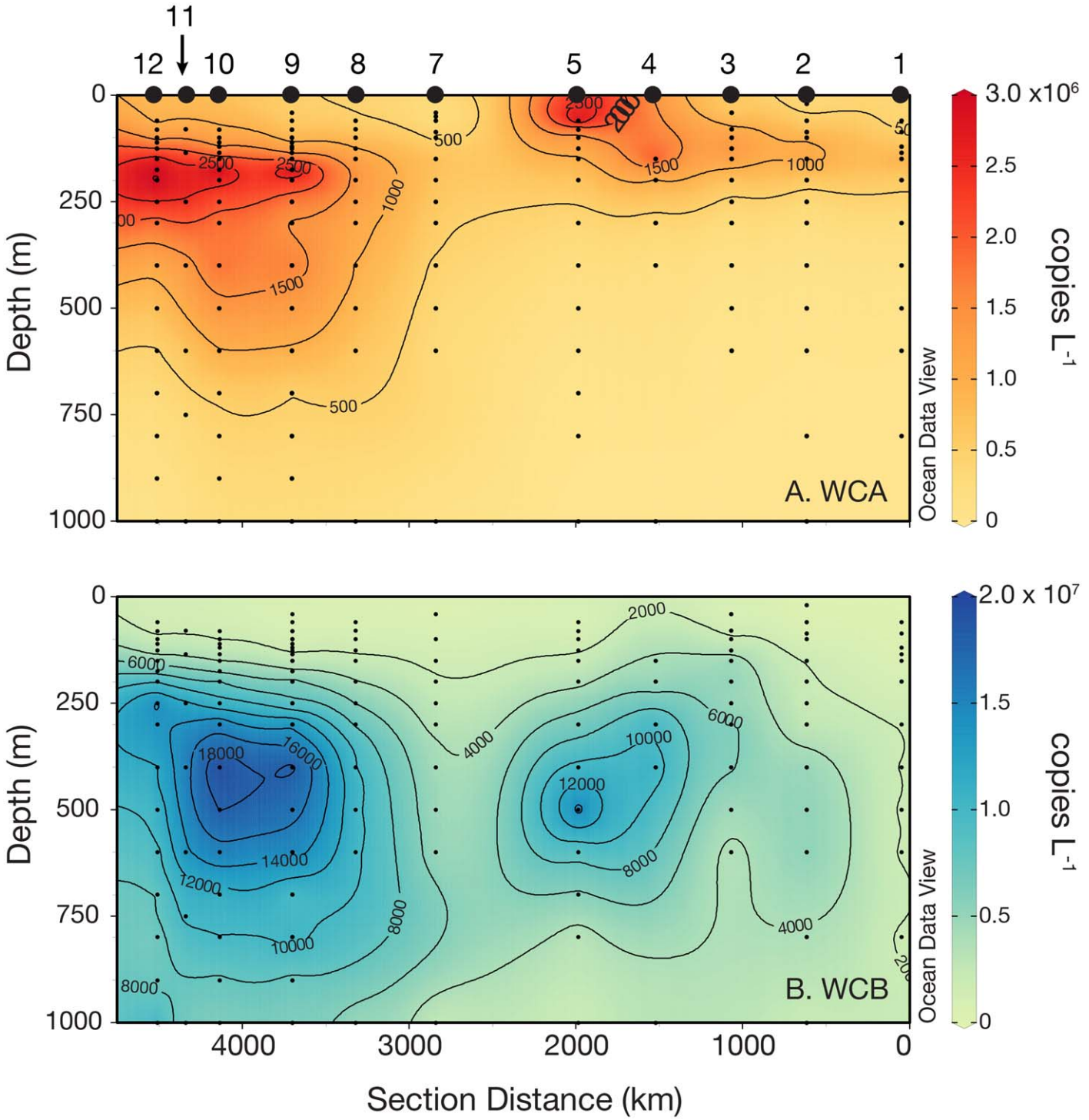

Fig. 4. Abundance of archaeal *amoA* genes in the equatorial Pacific between W. Samoa (section distance ~ 5000 km) and offshore of Hawai'i (section distance ~ 0 km) as determined by quantitative PCR (qPCR). (**A**) Water column "A" (WCA) clade, (**B**) water column "B" (WCB) clade. Station numbers are indicated along the top of panel **A**. Note the *x*-axis differs slightly from Fig. 1 to display data from multiple stations occupied along 15°S (see Fig. 1A), and that the color scale range is different for panels **A** and **B**. Points below the detection limit of our qPCR assays were coded as zero values for data interpolation using the weighted-average gridding algorithm in Ocean Data View v4.7.3 with automatic *x* and *y* scale lengths.

Table 2. Results of pairwise non-parametric correlation (Spearman's rho) between biological and physical parameters and ecotypes (WCA and WCB) of archaeal *amoA* genes. Bold text indicates *r* values supported by $p < 0.05$.

	WCA		WCB		
	r	*p*	*r*	*p*	
Depth	**−0.24**	0.00	**0.56**	0.00	CTD Sensor data
Temperature	**0.21**	0.01	**−0.57**	0.00	
Salinity	**0.28**	0.00	**−0.38**	0.00	
Oxygen (μmol/kg)	0.02	0.78	**−0.53**	0.00	
AOU* (μmol/kg)	–0.08	0.34	0.55	0.00	
Turbidity	−0.21	0.10	0.55	0.00	
Chlorophyll fluorescence	0.15	0.24	**−0.51**	0.00	
Conductivity (mS/cm)	**0.20**	0.02	**−0.54**	0.00	
Density	**−0.21**	0.01	0.59	0.00	
Potential density anomaly (σ_θ)	**−0.21**	0.01	0.58	0.00	
PO_4^{3-} (μM)	**−0.29**	0.00	0.51	0.00	Bottle measurements
N+N (μM)	**−0.28**	0.00	0.54	0.00	and derived variables
Silicate (μM)	**−0.34**	0.00	0.47	0.00	
NO_2^- (μM)	**0.27**	0.00	**−0.43**	0.00	
NH_4^+ (μM)	–0.19	0.05	–0.12	0.25	
NO_2:O_2	0.18	0.07	–0.16	0.12	
NO_3^- (μM)	**−0.29**	0.00	**0.54**	0.00	
NO_3:O_2	–0.15	0.14	**0.59**	0.00	
NO_3:Si	**0.58**	0.00	0.12	0.22	
Co (pM)	0.11	0.25	**0.42**	0.00	
% regenerated $NO_3^{-\dagger}$	**0.23**	0.03	0.11	0.31	
Total Hg (pM)	–0.03	0.77	**0.62**	0.00	
Hg_0 (pM)	**0.39**	0.00	–0.01	0.93	
% $Hg_0^{\ddagger}$	**0.29**	0.01	**−0.59**	0.00	
Dimethyl Hg (pM)	–0.09	0.49	**0.50**	0.00	
% Dimethyl Hg[§]	**0.25**	0.04	0.10	0.45	
Dissolved gaseous Hg (pM)	**0.37**	0.00	**0.33**	0.00	
% Dissolved gaseous Hg[‖]	**0.44**	0.00	**−0.45**	0.00	
WCA *amoA*	N.A.	N.A.	**0.24**	0.00	
Magnesium 2,4-divinylpheoporphyrin a_5 monomethyl ester (MgDVP)	–0.16	0.20	**−0.65**	0.00	HPLC pigments
Chl c_2	0.02	0.87	**−0.51**	0.00	
Chl c_1	0.06	0.65	**−0.43**	0.00	
Peridinin	**0.34**	0.01	0.07	0.59	
19′-Butanoyloxyfucoxanthin	**0.41**	0.03	**−0.55**	0.00	
Fucoxanthin	0.19	0.15	–0.07	0.60	
Neoxanthin	–0.08	0.53	**−0.42**	0.00	
Prasinoxanthin	0.05	0.71	–0.18	0.18	
Violaxanthin	**−0.36**	0.00	**−0.39**	0.00	
19′-Hexanoyloxyfucoxanthin	–0.01	0.91	**−0.45**	0.00	
Diadinoxanthin	–0.24	0.06	**−0.43**	0.00	
cis-Fucoxanthin	–0.08	0.54	–0.17	0.21	
Alloxanthin	**0.28**	0.03	–0.06	0.65	
Diatoxanthin	0.02	0.90	–0.17	0.20	
Monadoxanthin	0.15	0.24	–0.18	0.18	
Zeaxanthin	**−0.52**	0.00	**−0.63**	0.00	
Lutein	–0.24	0.06	–0.24	0.07	

TABLE 2. Continued

	WCA		WCB	
	r	*p*	*r*	*p*
β-8-Apocarotenal	**0.30**	0.02	0.21	0.12
Crocoxanthin	–0.09	0.50	**−0.32**	0.02
Chl c_2 like	0.22	0.08	0.08	0.57
Divinyl (DV) Chl *a*	**−0.30**	0.02	**−0.62**	0.00
Monovinyl (MV) Chl *a*	0.02	0.86	**−0.45**	0.00
Total Chl *a* (MV + DV)	–0.17	0.18	**−0.55**	0.00
β,ε-Carotene	**0.30**	0.02	–0.05	0.73
β,β-Carotene	0.22	0.08	0.02	0.91
Chl c_3	**0.31**	0.02	–0.25	0.06
Chl *b*	0.25	0.05	**−0.41**	0.00
Chlorophyllide *a*	0.10	0.44	–0.08	0.57
Phaeophorbide *a*	0.00	0.98	**−0.45**	0.00
Phaeophytin *a*	0.06	0.79	**−0.63**	0.00

* Apparent oxygen utilization.
† Regenerated NO_3^- calculated using AOU and the respiration stoichiometry of Anderson (1995) (i.e., AOU/10.6), reported as a percent of total $[NO_3^-]$.
‡,§,|| As a percent of total Hg.

56 variables included in the analysis, only $[NO_2^-]$ was retained in the final model for WCA abundance.

WCB *amoA* genes were also near or below detection limits in the euphotic zone. In contrast to WCA *amoA* genes, however, WCB *amoA* depth profiles had increasing abundance through the upper mesopelagic (Fig. 2C,F), and were detectible down to the deepest depth sampled at every station (1000 m, or 3000 m at stations 5 and 9). As mentioned above, WCB *amoA* genes were observed in very high abundance within a mesopelagic feature spanning stations 9–12 (Fig. 4B). Within this feature, WCB *amoA* abundance reached 4.5×10^7 genes L^{-1} (station 10, 400 m depth). WCB *amoA* abundance was significantly correlated with nearly every physicochemical parameter measured (Table 2), owing to a strong correlation between WCB *amoA* abundance and depth ($r = 0.56$, $p < 0.001$) and the co-variation with depth of most physicochemical parameters. Therefore, a partial correlation analysis, controlling for depth, was also carried out to evaluate factors controlling WCB *amoA* abundance (Table 3). Strongest partial correlations were found with indicators of remineralization: total Hg ($r = 0.44$, $p < 0.001$), dimethyl Hg ($r = 0.43$, $p < 0.001$), dissolved cobalt ($r = 0.37$, $p < 0.001$), NO_3 : Si ($r = 0.38$, $p < 0.001$), AOU ($r = 0.25$, $p < 0.01$), and fraction remineralized NO_3^- ($r = 0.25$, $p = 0.02$). WCB abundance was not successfully modeled using stepwise regression. High abundances of WCB *amoA* genes were observed underlying waters with relatively high abundances of WCA *amoA* genes (Fig. 4); depth-integrated abundances of WCA and WCB *amoA* genes were strongly correlated ($r = 0.82$, $p < 0.01$, $n = 11$), more so than pairwise correlation of individual samples ($r = 0.24$, $p < 0.01$, $n = 145$).

In addition to correlations between the absolute abundance of the ecotypes, we also investigated physical factors that may govern community structure and the shift from a WCA-dominated to a WCB-dominated community by examining the percent of total *amoA* genes belonging to the WCB clade (%WCB; Fig. 5). Plotting %WCB with respect to seawater density shows a relatively sharp boundary around $\sigma_T = 26$ kg m^{-3}. Plotted against the depth-dependent variables temperature and phosphate (also a proxy for many micronutrients), there is considerable scatter around the transition from a WCA to a WCB-dominated community (Fig. 5C,D).

Thaumarchaeal gene content in metagenomes

Metgenomic libraries were constructed from samples collected at stations 3 and 5 at depths from 50 m to 800 m (Table 4; Supporting Information Table S3). Thaumarchaeal *amoA*, *amtB*, and *ureC* genes were detected in all samples (Table 4), but no hits to thaumarchaeal photolyase were detected. Contigs containing a thaumarchaeal 16S rRNA, *amoA* and/or *ureC* gene represented 0.003–0.013% of the total assembled sequence data (Supporting Information Table S3). Average fold coverage of these contigs in the raw data was highest in the 550 m and 800 m libraries (Fig. 6). The ratio of *ureC* : *amoA* in each sample ranged from 0.22 (800 m) to 0.55 (50 m), indicating that up to 55% of *amoA*-containing thaumarchaeal genomes also contain *ureC*.

Depth partitioning was apparent in *amoA* sequences retrieved from the metagenome (Supporting Information Fig. S1A). Two WCA clade *amoA* sequences were recovered from station 5, 50 m and station 3, 150 m libraries forming a monophyletic clade with *Ca*. N. brevis CN25, distinct from

Table 3. Results of partial non-parametric correlation (Spearman's rho) between biological and physical parameters and ecotypes (WCA and WCB) of archaeal *amoA* genes, controlling for depth. Bold text indicates *r* values supported by $p < 0.05$.

	WCA		WCB	
	r	***p***	***r***	***p***
Temperature	−0.02	0.79	−0.08	0.37
Salinity	**0.17**	0.04	−0.06	0.48
Oxygen (μmol/kg)	**–0.17**	0.04	**–0.31**	0.00
AOU* (μmol/kg)	0.13	0.14	**0.25**	0.00
Turbidity	0.05	0.68	**0.26**	0.04
Chlorophyll fluorescence	−0.12	0.34	**–0.25**	0.05
Conductivity (mS/cm)	0.00	0.96	−0.03	0.73
Density	0.07	0.39	0.10	0.25
Potential density anomaly (σ_θ)	0.06	0.45	0.09	0.29
PO_4^{3-} (μM)	0.02	0.85	**0.24**	0.02
N+N (μM)	0.06	0.52	**0.27**	0.01
Silicate (μM)	−0.02	0.81	0.06	0.51
NO_2^- (μM)	0.13	0.18	**–0.23**	0.02
NH_4^+ (μM)	**–0.23**	0.02	−0.14	0.16
NO_2:O_2	0.12	0.23	0.01	0.95
NO_3^- (μM)	0.06	0.54	**0.27**	0.00
NO_3:O_2	0.13	0.21	**0.39**	0.00
NO_3:Si	**0.54**	0.00	**0.38**	0.00
Co (pM)	**0.27**	0.01	**0.37**	0.00
% Regenerated $NO_3^{-\dagger}$	0.01	0.91	**0.25**	0.02
Total Hg (pM)	**0.23**	0.04	**0.44**	0.00
Hg_0 (pM)	**0.42**	0.00	0.11	0.32
% $Hg_0^{\ddagger}$	0.13	0.26	**–0.27**	0.02
Dimethyl Hg (pM)	**0.27**	0.03	**0.43**	0.00
% Dimethyl Hg[§]	**0.28**	0.02	0.17	0.18
Dissolved gaseous Hg (pM)	**0.49**	0.00	**0.36**	0.00
% Dissolved gaseous Hg[‖]	**0.35**	0.00	−0.04	0.71
Magnesium 2,4-divinylpheoporphyrin a_5 monomethyl ester (MgDVP)	0.08	0.54	**–0.37**	0.00
Chl c_2	**0.32**	0.01	−0.16	0.21
Chl c_1	**0.33**	0.01	−0.10	0.45
Peridinin	**0.56**	0.00	**0.42**	0.00
19′-Butanoyloxyfucoxanthin	**0.65**	0.00	0.00	0.99
Fucoxanthin	**0.43**	0.00	**0.35**	0.01
Neoxanthin	0.22	0.09	−0.10	0.43
Prasinoxanthin	0.07	0.62	−0.16	0.21
Violaxanthin	−0.14	0.29	−0.20	0.12
19′-Hexanoyloxyfucoxanthin	**0.30**	0.02	−0.07	0.60
Diadinoxanthin	**0.27**	0.04	0.19	0.15
cis-Fucoxanthin	−0.04	0.74	−0.12	0.36
Alloxanthin	**0.52**	0.00	**0.34**	0.01
Diatoxanthin	**0.37**	0.00	0.20	0.12
Monadoxanthin	**0.30**	0.02	0.06	0.62
Zeaxanthin	−0.22	0.09	−0.18	0.17
Lutein	−0.15	0.26	−0.06	0.65
β-8-Apocarotenal	**0.41**	0.00	**0.53**	0.00
Crocoxanthin	0.22	0.08	0.10	0.44

TABLE 3. Continued

	WCA		WCB	
	r	*p*	*r*	*p*
Chl c_2 like	**0.39**	0.00	**0.39**	0.00
Divinyl (DV) Chl *a*	−0.05	0.72	**–0.33**	0.01
Monovinyl (MV) Chl *a*	**0.30**	0.02	−0.16	0.23
Total Chl *a* (MV + DV)	0.12	0.37	−0.23	0.07
β,ε-Carotene	**0.49**	0.00	**0.28**	0.03
β,β-Carotene	**0.38**	0.00	**0.39**	0.00
Chl c_3	**0.55**	0.00	0.13	0.32
Chl *b*	**0.41**	0.00	−0.16	0.21
Chlorophyllide *a*	**0.31**	0.02	**0.29**	0.03
Phaeophorbide *a*	0.18	0.16	−0.25	0.05
Phaeophytin *a*	0.09	0.50	**–0.43**	0.00

* Apparent oxygen utilization.
† Regenerated NO_3^- calculated using AOU and the respiration stoichiometry of Anderson (1995) (i.e., AOU/10.6), reported as a percent of total [NO_3^-].
‡,§,‖ As a percent of total Hg.

Table 4. Genotype counts for select thaumarchaeal genes identified in the assembled metagenomes, used for determining coverage values shown in Fig. 6.

Station	Depth (m)	*amoA*	*amtB1*	*ureC*
5	50	1	2	1
3	150	5	4	1
3	250	5	3	1
3	300	7	2	2
3	550	5	4	1
3	800	5	3	2

the WCB *amoA* sequences found deeper in the water column. *amoA* diversity was greater within the WCB clade, but similar sequences were found at 150 m and 800 m depth. One *ureC* sequence type apparently affiliated with the WCA clade was found in the station 5, 50 m library, falling within a clade including cultivated thaumarchaea (Supporting Information Fig. S2B).

Discussion

The aim of this study was to understand the physicochemical controls on the abundance and partitioning of two presumptive ecotypes of ammonia-oxidizing thaumarchaea at the basin scale, and quantify nitrification in the equatorial Pacific, a site of intensive previous studies of nitrogen cycling (Wilkerson and Dugdale 1992; Raimbault et al. 1999) and organic matter export (Murray et al. 1995). Nitrification rates at station 1 and station 5 displayed a characteristic power law profile (Ward 2008; Newell et al. 2011; Smith et al. 2015), with highest rates just below the DCM, decreasing exponentially below (Fig. 2B,E). This was not observed at station 3, where high rates of nitrification near the base of the euphotic zone were not captured (Supporting Information Table S1). Loss of the real-time output on the CTD sensor for stations 2–4 prevented choosing precise incubation depths relative to the Chl *a* maximum at station 3, so it is likely this narrow maximum in nitrification rates was missed by our sampling. Our data are qualitatively consistent with previously observed distributions of nitrification rates in the water column of the tropical Pacific (Ward and Zafiriou 1988; Raimbault et al. 1999; Beman et al. 2012) and other oceanic regions (Clark et al. 2008; Newell et al. 2013) and provide the first rate measurements of sub-euphotic zone nitrification in this region.

Nitrification is the final step of nitrogen remineralization in the breakdown of organic matter, thus, the depth-integrated nitrification rate should be directly related to organic nitrogen (and carbon) export from the base of the euphotic zone. Surprisingly, there are limited direct comparisons of these two measurements from a single expedition. As mentioned above, the PAR sensor was lost during sampling at station 2, thus direct light measurements with which to calculate euphotic zone depth were not possible for most of the cruise. If we take the depth of the DCM, however, to approximate the 1% light depth as it does throughout much of the oligotrophic ocean (Cullen 2015) and depth-integrate nitrification rates between there and 300 m, we arrive at 0.39 mmol m^{-2} d^{-1} at station 1, 0.92 mmol m^{-2} d^{-1} at station 3, and 2.17 mmol m^{-2} d^{-1} at station 5 (Table 1). These values compare well with, though are somewhat higher than, previous estimates of N export from the equatorial Pacific [0.76 mmol m^{-2} d^{-1} (Dugdale and Wilkerson 1998); 0.88 mmol m^{-2} d^{-1} (Chai et al. 2002)]. Depth-integrated nitrification rates were correlated with both depth-integrated Chl *a* ($R^2 = 0.96$) and sediment trap PON export at 60 m ($R^2 = 0.94$), the later reported by Munson et al. (2015).

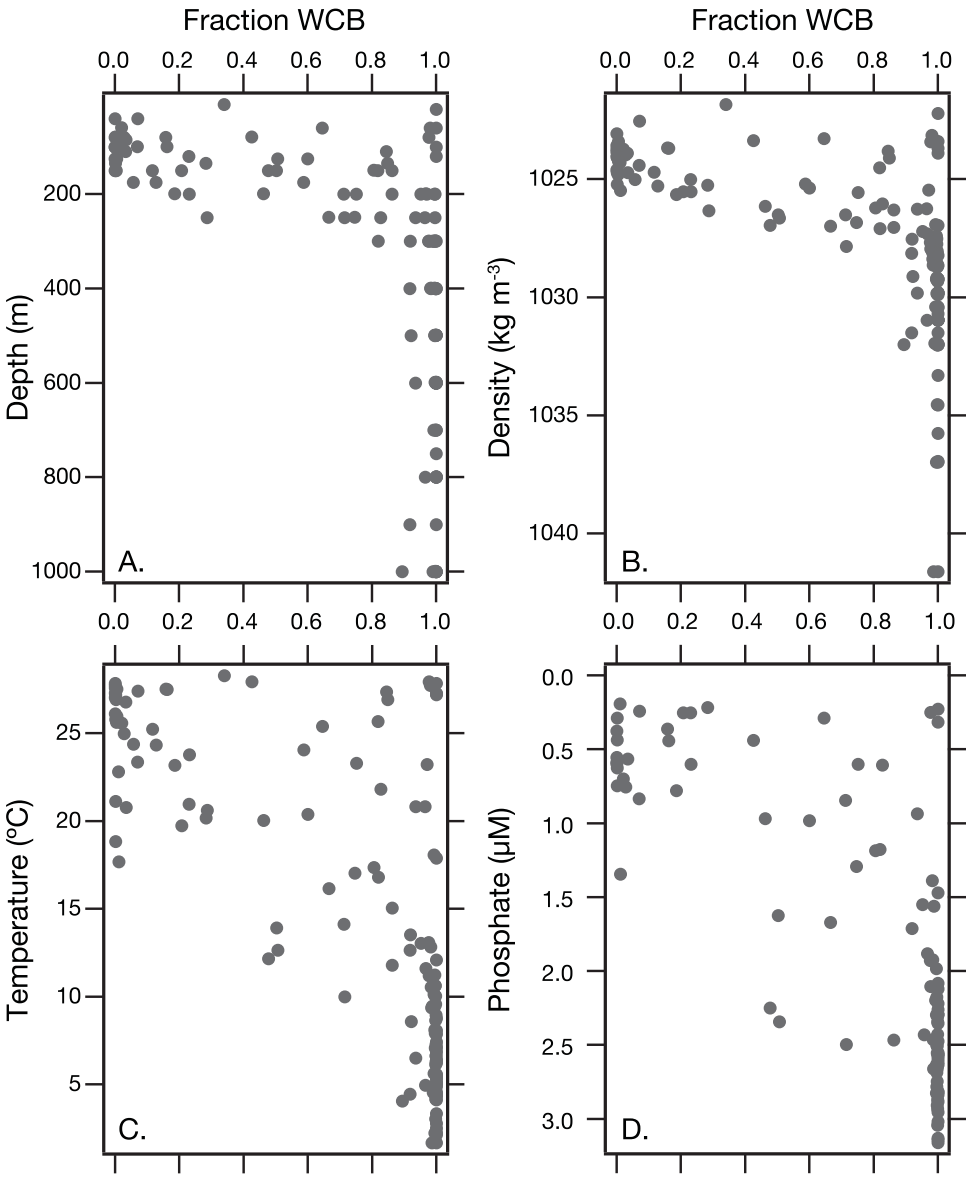

Fig. 5. Fraction of total *amoA* genes belonging to the water column B clade as a function of (**A**) depth, (**B**) seawater density, (**C**) temperature, and (**D**) inorganic phosphate concentration.

Previous studies in the Pacific have found positive correlations between depth-integrated primary production and nitrification (Beman et al. 2012; Shiozaki et al. 2016). The correlations in our data and others support a direct and quantitative connection between nitrification rates, euphotic zone biomass, and PON export (Newell et al. 2011).

Rates of nitrification and coupled urea hydrolysis-nitrification were similar, and suggest that urea could be an important source of NH_3 fueling nitrification in the mesopelagic as has been recently shown in mesopelagic waters over the Antarctic Shelf (Tolar et al. 2016). Our experiments cannot resolve whether this transformation is being carried out by a single group of organisms, or a consortium of urea-hydrolyzing microbes and ammonia oxidizers, as was recently proposed (Koch et al. 2015). Cultures of urea-utilizing marine ammonia-oxidizing archaea have been reported (Qin et al. 2014; Bayer et al. 2015) and urease genes have been detected in multiple cultivation-independent studies of marine thaumarchaea (Alonso-Saez et al. 2012; Tully et al. 2012; Swan et al. 2014). Here, thaumarchaeal *ureC* genes were detected in metagenomes at all depths, suggesting that both ecotypes of thaumarchaea may possess the ability to use urea as a source of NH_3. A recent study, however, did not find evidence of thaumarchaeal *ureC* expression in the mesopelagic though *ureC* genes were detected (Smith et al. 2015). While it has been suggested that urease may be a

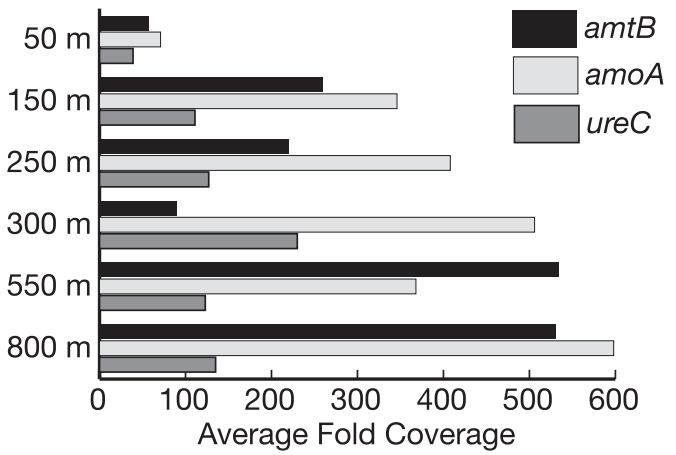

Fig. 6. Average fold coverage of select thaumarchaeal genes in six metagenomes from the equatorial Pacific. Average fold coverage is the average number of times a base pair in the given gene is covered by a sequencing read. All samples are from station 3, except the 50 m sample which is from station 5.

feature of coastal thaumarchaea (Bayer et al. 2015), the distribution of *ureC* genes and degradation rates reported here suggest it may also be an important substrate for nitrogen remineralization in the open ocean (Cho and Azam 1995).

Nitrification was inhibited by the metal chelator TETA, as would be expected for a group of organisms with abundant metalloenzymes involved in energy metabolism (Walker et al. 2010; Santoro et al. 2015). In the only study to date to specifically examine the metal requirements of ammonia-oxidizing archaea, *Nitrosopumilus maritimus* SCM1 was found to be limited at $[Cu^{2+}]$ below 10^{-13} mol L^{-1} (Amin et al. 2013). Here, nitrification rates at 150 m showed less inhibition by TETA than rates at 300 m, when expressed as a percent of the uninhibited rate (Fig. 3A). The greater inhibition of the deeper nitrifying community is somewhat surprising given that many biologically active metals (including Fe and Cu) display nutrient-like characteristics, with low concentrations in the photic zone and increased concentrations at depth from remineralization (Bruland and Lohan 2003). One potential explanation for the results presented here is that TETA-induced inhibition of nitrification was the result not of Fe or Cu binding, but instead cobalt (Co) binding. Co has a "hybrid" profile, with highest concentrations in the upper mesopelagic, but lower concentrations above and below due to phytoplankton uptake and particle scavenging, respectively (Noble et al. 2008). At station 3, [Co] was 123 pM at 150 m, but only 70 pM at 300 m (Saito et al. 2014). TETA has a strong affinity for Co; thermodynamic stability constants show an affinity for metals in the order Cu, Co, Ni, Zn, Fe(III), and Fe(II) (Martell and Smith 1977). Hence, the combination of decreased Co concentration at depth and addition of TETA could explain the observations here. Differences in metal affinities among the shallow and deep ecotypes of ammonia-oxidizing archaea (AOA) may also partially explain our observations. Fifteen percent of the thaumarchaea at 150 m were from the shallow WCA clade, compared with $< 1\%$ at 300 m. If the WCA clade has a higher affinity for a bioactive trace metal, they may be able to access trace metals even in the presence of a strong binding ligand, resulting in less relative inhibition at shallower depths. Finally, the presence of different metal binding ligands naturally occurring in the water column at 150 m and 300 m with different relative stability constants may also play a role in the differential inhibition at different depths.

The overall depth distribution of thaumarchaea observed here—low abundances throughout the euphotic zone, peak abundance in the upper mesopelagic, and slightly decreased abundance below—is similar to previous reports of thaumarchaeal distributions in the ocean (Karner et al. 2001; Herndl et al. 2005; Newell et al. 2013). Church et al. (2010) mapped the abundance of thaumarchaeal *amoA* genes across the equatorial Pacific slightly west of our transect, finding the highest mesopelagic *amoA* abundances near the Equator, at 3.0°S and 1.7°N. Total *amoA* abundances here, calculated as the sum of WCA and WCB *amoA* genes, agree surprisingly well with the Church et al. study, given the inherent variability of sampling microorganisms in the ocean and the differences in qPCR assays used between the two studies. For example, depth-averaged *amoA* abundance between 300 m and 1000 m at station 2 (2.5×10^6 genes L^{-1}) is nearly identical to that calculated by Church et al. at 13.5°N (2.3×10^6 copies L^{-1}) over the same interval, implying that the WCA and WCB distributions observed here are broadly characteristic of the equatorial Pacific through time.

The WCA ecotype appears to be responsible for the high rates of ammonia oxidation at the top of the nitracline. At stations where nitrification rates were determined, WCA *amoA* genes were abundant at the same depth as the nitrification rate maximum (Fig. 2), where few WCB genes were found, and were inversely correlated with $[NH_4^+]$, suggesting they are a sink for NH_4^+. WCA *amoA* genes were also strongly correlated with geochemical tracers of remineralization, in particular NO_3 : Si, an indication of the shorter remineralization length scale of N vs. Si in this region (Raimbault et al. 1999; Jiang et al. 2003; Buesseler et al. 2008) and/or the remineralization of non-diatomaceous organic matter. These results support previous findings that WCA *amoA* genes are correlated with nitrification rates in a temporal study in Monterey Bay, California (Smith et al. 2014) and NO_3 : Si (Smith et al. 2015). As these depths are associated with the highest nitrification rates, we suggest members of the WCA clade are responsible for most of the ammonia oxidation in the ocean. This high activity appears to be catalyzed by a relatively low diversity of WCA *amoA* genes in the 50 m metagenome (Supporting Information Fig. S1), though this may

be influenced by the relatively low sequence coverage of thaumarchaea at this depth.

Our data are equivocal in identifying the causes of a transition from a WCA-dominated to a WCB-dominated thaumarchaeal community. While temperature is an important master variable in the ecology of other marine microbes (Zubkov et al. 2000), this was not observed here. Similarly, though oxygen has previously been observed to influence the composition of *amoA*-containing thaumarchaea (Bouskill et al. 2012), and here is negatively correlated with both WCA and WCB abundance, it does not appear to be the primary driver of the ecotype division. We did, however, observe a relatively sharp transition at approximately the $\sigma_t = 26$ kg m^{-2} isopycnal, just below the euphotic zone and at the maximum NO3 : Si, suggesting that niche differentiation between the WCA and WCB ecotypes may be driven by substrate (ammonium) flux. These data support the observations of Sintes et al. (2013, 2015, 2016) and Smith et al. (2015), who suggested that the shallow and deep ecotypes are adapted to "high" and "low" ammonium concentrations, respectively. We posit, however, it is not ammonium concentration, but rather ammonium flux, through these depths that is more likely a driver of niche differentiation, as [NH_4^+] in our dataset is below 120 nM at all depths. It should also be noted that the availability of other remineralization products that could contribute to growth of ammonia oxidizers (trace metals, amino acids, or other organic compounds) would also be high at these depths, which could contribute to selection for the shallow ecotype at the depths of the highest remineralization rates.

If differentiation between the WCA and WCB ecotypes is, in fact, related to NH_3/NH_4^+ flux, it may also be the result of differences in affinity for NH_4^+ for assimilation, not oxidation. The extended N-terminus of the AmtB-1 protein in thaumarchaea contains a large number of negatively charged residues, which may contribute to NH_4^+ affinity (Offre et al. 2014). Despite the depth partitioning of AmtB-1 observed here (Supporting Information Fig. S2), we found no differences in the number of negatively charged residues in the predicted N-terminus loop structure between shallow and deep sequences, and the three hypothesized NH_4^+ binding residues are conserved in these sequences as they are in all thaumarchaea (Offre et al. 2014).

The correlation between the depth-integrated inventory of WCA and WCB ecotypes suggests the abundance of WCB organisms in deep mesopelagic waters is linked to processes occurring shallower in the water column, as has been suggested by previous diversity-based investigations of AOA (Sintes et al. 2015) and is apparent in the quantitative data of Church et al. (2010). While this result may seem somewhat intuitive, few studies have examined potential correlations between microbial abundance in the epipelagic and mesopelagic across the spatial scales examined here. Nagata et al. (2000) found a correlation both between epipelagic phytoplankton biomass and mesopelagic microbial biomass, and mesopelagic and bathypelagic microbial biomass in the Pacific. Arístegui et al. (2009) found similar correlations in a synthesis of available microbial cell count data. Yet, in the Arabian Sea, contemporaneous measures of POC and microbial standing stocks were not correlated, but were when considering annual averages of export (Hansell and Ducklow 2003). Here, we found that the water column inventory of the WCB ecotype through the lower mesopelagic was linearly related to POC and PON flux at 60 m ($R^2 = 0.99$, $n = 3$) across a strong gradient in export flux.

Others have argued that water mass history is the primary determinant of microbial community structure in the mesopelagic (Reinthaler et al. 2010). Our data instead indicate that mesopelagic microbial communities, in fact, retain the imprint of material export from the surface. Waters in the 400–600 m depth range along the cruise track south of the Equator originate from the same source waters, predominantly Subantarctic Mode Water (Rafter et al. 2012, and references therein), thus it seems unlikely that water mass origin is the primary determinant of the large variations in WCB abundance we observed across the study area. Instead, our data contribute to a growing demonstration of the connection between surface and mesopelagic microbial communities (Cram et al. 2015; Frank et al. in press). The extent to which a quantitative approach to mesopelagic community structure can inform our quantitative understanding of POC and PON export from the surface is an area for future research.

References

Alonso-Saez, L., and others. 2012. Role for urea in nitrification by polar marine Archaea. Proc. Natl. Acad. Sci. USA **109**: 17989–17994. doi:10.1073/Pnas.1201914109

Amin, S. A., and others. 2013. Copper requirements of the ammonia-oxidizing archaeon *Nitrosopumilus maritimus* SCM1 and implications for nitrification in the marine environment. Limnol. Oceanogr. **58**: 2037–2045. doi:10.4319/Lo.2013.58.6.2037

Anderson, L. A. 1995. On the hydrogen and oxygen content of marine phytoplankton. Deep-Sea Res. I **42**: 1675–1680. doi:10.1016/0967-0637(95)00072-E

Arístegui, J., J. M. Gasol, C. M. Duarte, and G. J. Herndl. 2009. Microbial oceanography of the dark ocean's pelagic realm. Limnol. Oceanogr. **54**: 1501–1529. doi:10.4319/lo.2009.54.5.1501

Bayer, B., and others. 2015. Physiological and genomic characterization of two novel marine thaumarchaeal strains indicates niche differentiation. ISME J. **10**: 1051–1063. doi:10.1038/ismej.2015.200

Beman, J. M., N. Popp, and C. A. Francis. 2008. Molecular and biogeochemical evidence for ammonia oxidation by marine Crenarchaeota in the Gulf of California. ISME J. **2**: 429–441. doi:10.1038/ismej.2007.118

Beman, J. M., N. Popp, and S. E. Alford. 2012. Quantification of ammonia oxidation rates and ammonia-oxidizing archaea and bacteria at high resolution in the Gulf of California and eastern tropical North Pacific Ocean. Limnol. Oceanogr. **57**: 711–726. doi:10.4319/lo.2012.57.3.0711

Biller, S. J., C. Mosier, G. F. Wells, and C. A. Francis. 2012. Global biodiversity of aquatic ammonia-oxidizing archaea is partitioned by habitat. Front. Microbiol. **3**. doi:10.3389/Fmicb.2012.00252

Bouskill, N. J., D. Eveillard, D. Chien, A. Jayakumar, and B. B. Ward. 2012. Environmental factors determining ammonia-oxidizing organism distribution and diversity in marine environments. Environ. Microbiol. **14**: 714–729. doi:10.1111/j.1462-2920.2011.02623.x

Bruland, K. W., and M. C. Lohan. 2003. Controls of trace metals in seawater. *In* H. D. Holland and K. K. Turekian [eds.], Treatise on geochemistry. Elsevier Science Ltd.

Buesseler, K. O., and others. 2008. VERTIGO (VERtical Transport in the Global Ocean): A study of particle sources and flux attenuation in the North Pacific. Deep-Sea Res. **55**: 1522–1539. doi:10.1016/J.Dsr2.2008.04.024

Carlson, C. A., R. Morris, R. Parsons, A. H. Treusch, S. J. Giovannoni, and K. Vergin. 2009. Seasonal dynamics of SAR11 populations in the euphotic and mesopelagic zones of the northwestern Sargasso Sea. ISME J. **3**: 283–295. doi:10.1038/Ismej.2008.117

Chai, F., R. C. Dugdale, T. H. Peng, F. P. Wilkerson, and R. T. Barber. 2002. One-dimensional ecosystem model of the equatorial Pacific upwelling system. Part I: Model development and silicon and nitrogen cycle. Deep-Sea Res. Part II **49**: 2713–2745. doi:10.1016/S0967-0645(02)00055-3

Cho, B. C., and F. Azam. 1988. Major role of bacteria in biogeochemical fluxes in the ocean's interior. Nature **332**: 441–443. doi:10.1038/332441a0

Cho, B. C., and F. Azam. 1995. Urea decomposition by bacteria in the Southern California Bight and its implications for the mesopelagic nitrogen cycle. Mar. Ecol. Prog. Ser. **122**: 21–26. doi:10.3354/meps122021

Church, M. J., M. Karl, and E. F. Delong. 2010. Abundances of crenarchaeal *amoA* genes and transcripts in the Pacific Ocean. Environ. Microbiol. **12**: 679–688. doi:10.1111/j.1462-2920.2009.02108.x

Clark, D. R., P. Rees, and I. Joint. 2008. Ammonium regeneration and nitrification rates in the oligotrophic Atlantic Ocean: Implications for new production estimates. Limnol. Oceanogr. **53**: 52–62. doi:10.4319/lo.2008.53.1.0052

Cohan, F. M. 2001. Bacterial species and speciation. Syst. Biol. **50**: 513–524. doi:10.1080/10635150118398

Cordero, O. X., and M. F. Polz. 2014. Explaining microbial genomic diversity in light of evolutionary ecology. Nat. Rev. Microbiol. **12**: 263–273. doi:10.1038/nrmicro3218

Cram, J. A., L. C. Xia, D. M. Needham, R. Sachdeva, F. Z. Sun, and J. A. Fuhrman. 2015. Cross-depth analysis of marine bacterial networks suggests downward propagation of temporal changes. ISME J. **9**: 2573–2586. doi:10.1038/ismej.2015.76

Cullen, J. J. 2015. Subsurface chlorophyll maximum layers: Enduring enigma or mystery solved? Ann. Rev. Mar. Sci. **7**: 207–239. doi:10.1146/annurev-marine-010213-135111

Dugdale, R. C., and J. J. Goering. 1967. Uptake of new and regenerated forms of nitrogen in primary productivity. Limnol. Oceanogr. **12**: 196–206. doi:10.4319/lo.1967. 12.2.0196

Dugdale, R. C., and F. P. Wilkerson. 1998. Silicate regulation of new production in the equatorial Pacific upwelling. Nature **391**: 270–273. doi:10.1038/34630

Dupont, C. L., and others. 2012. Genomic insights to SAR86, an abundant and uncultivated marine bacterial lineage. ISME J. **6**: 1186–1199. doi:10.1038/ismej.2011.189

Follows, M. J., S. Dutkiewicz, S. Grant, and S. W. Chisholm. 2007. Emergent biogeography of microbial communities in a model ocean. Science **315**: 1843–1846. doi:10.1126/Science.1138544

Francis, C. A., J. Roberts, J. M. Beman, A. E. Santoro, and B. B. Oakley. 2005. Ubiquity and diversity of ammonia-oxidizing archaea in water columns and sediments of the ocean. Proc. Natl. Acad. Sci. USA **102**: 14683–14688. doi:10.1073/pnas.0506625102

Frank, A., J. Garcia, G. Herndl, and T. Reinthaler. 2015. Connectivity between surface and deep waters determines prokaryotic diversity in the North Atlantic Deep Water. Environ. Microbiol. **18**: 2052–2063. doi:10.1111/1462-2920.13237

Glibert, P., F. Lipschultz, J. Mccarthy, and M. Altabet. 1982. Isotope dilution models of uptake and remineralization of ammonium by marine plankton. Limnol. Oceanogr. **27**: 639–650. doi:10.4319/lo.1982.27.4.0639

Gruber, N. 2008. The marine nitrogen cycle: Overview and challenges, p. 1–50. In D. G. Capone, D. A. Bronk, M. R. Mulholland and E. J. Carpenter [eds.], Nitrogen in the marine environment. Elsevier.

Hallam, S. J., J. Mincer, C. Schleper, C. M. Preston, K. Roberts, P. M. Richardson, and E. F. Delong. 2006. Pathways of carbon assimilation and ammonia oxidation suggested by environmental genomic analyses of marine Crenarchaeota. PLoS Biol. **4**: 520–536. doi:10.1371/journal.pbio.0040437

Hansell, D. A., and H. W. Ducklow. 2003. Bacterioplankton distribution and production in the bathypelagic ocean: Directly coupled to particulate organic carbon export? Limnol. Oceanogr. **48**: 150–156. doi:10.4319/lo.2003.48.1.0150

Herndl, G. J., T. Reinthaler, E. Teira, H. Van Aken, C. Veth, A. Pernthaler, and J. Pernthaler. 2005. Contribution of Archaea to total prokaryotic production in the deep Atlantic Ocean. Appl. Environ. Microbiol. **71**: 2303–2309. doi:10.1128/aem.71.5.2303-2309.2005

Holmes, R. M., A. Aminot, R. Kèrouel, B. A. Hooker, and B. J. Peterson. 1999. A simple and precise method for measuring ammonium in marine and freshwater ecosystems. Can. J. Fish. Aquat. Sci. **56**: 1801–1808. doi:10.1139/cjfas-56-10-1801

Horak, R. E. A., W. Qin, A. J. Shauer, E. V. Armbrust, A. E. Ingalls, J. W. Moffett, D. A. Stahl, and A. H. Devol. 2013. Ammonia oxidation kinetics and temperature sensitivity of a natural marine community dominated by Archaea. ISME J. **7**: 2023–2033. doi:10.1038/ismej.2013.75

Jiang, M. S., F. Chai, R. C. Dugdale, F. P. Wilkerson, T. H. Peng, and R. T. Barber. 2003. A nitrate and silicate budget in the equatorial Pacific Ocean: A coupled physical-biological model study. Deep-Sea Res. **50**: 2971–2996. doi:10.1016/j.dsr2.2003.07.006

Johnson, Z. I., R. Zinser, A. Coe, N. P. Mcnulty, E. M. S. Woodward, and S. W. Chisholm. 2006. Niche partitioning among *Prochlorococcus* ecotypes along ocean-scale environmental gradients. Science **311**: 1737–1740. doi:10.1126/science.1118052

Karner, M. B., F. Delong, and D. M. Karl. 2001. Archaeal dominance in the mesopelagic zone of the Pacific Ocean. Nature **409**: 507–510. doi:10.1038/35054051

Katoh, K., and D. M. Standley. 2013. MAFFT multiple sequence alignment software version 7: Improvements in performance and usability. Mol. Biol. Evol. **30**: 772–780. doi:10.1093/molbev/mst010

Koch, H., and others. 2015. Expanded metabolic versatility of ubiquitous nitrite-oxidizing bacteria from the genus *Nitrospira*. Proc. Natl. Acad. Sci. USA **112**: 11371–11376. doi:10.1073/pnas.1506533112

Könneke, M., A. E. Bernhard, J. R. D. La Torre, C. B. Walker, J. B. Waterbury, and D. A. Stahl. 2005. Isolation of an autotrophic ammonia-oxidizing marine archaeon. Nature **437**: 543–546. doi:10.1038/nature03911

Lamborg, C. H., and others. 2014. A global ocean inventory of anthropogenic mercury based on water column measurements. Nature **512**: 65–68. doi:10.1038/nature13563

Larsson, A. 2014. AliView: A fast and lightweight alignment viewer and editor for large datasets. Bioinformatics **30**: 3276–3278. doi:10.1093/bioinformatics/btu531

Luo, H. W., B. Tolar, B. K. Swan, C. L. L. Zhang, R. Stepanauskas, M. A. Moran, and J. T. Hollibaugh. 2014. Single-cell genomics shedding light on marine Thaumarchaeota diversification. ISME J. **8**: 732–736. doi:10.1038/ismej.2013.202

Malmstrom, R. R., A. Coe, G. C. Kettler, A. C. Martiny, J. Frias-Lopez, E. R. Zinser, and S. W. Chisholm. 2010. Temporal dynamics of *Prochlorococcus* ecotypes in the Atlantic and Pacific oceans. ISME J. **4**: 1252–1264. doi:10.1038/Ismej.2010.60

Martell, A. E., and R. M. Smith. 1977. Critical stability constants. Plenum Press.

Martens-Habbena, W., P. M. Berube, H. Urakawa, J. R. De La Torre, and D. A. Stahl. 2009. Ammonia oxidation kinetics determine niche separation of nitrifying Archaea and Bacteria. Nature **461**: 976–981. doi:10.1038/nature08465

Mcilvin, M. R., and K. L. Casciotti. 2011. Technical updates to the bacterial method for nitrate isotopic analyses. Anal. Chem. **83**: 1850–1856. doi:10.1021/ac1028984

Mincer, T. J., J. Church, L. T. Taylor, C. Preston, D. M. Karl, and E. F. Delong. 2007. Quantitative distribution of presumptive archaeal and bacterial nitrifiers in Monterey Bay and the North Pacific Subtropical Gyre. Environ. Microbiol. **9**: 1162–1175. doi:10.1111/j.1462-2920.2007. 01239.x

Moore, L. R., G. Rocap, and S. W. Chisholm. 1998. Physiology and molecular phylogeny of coexisting *Prochlorococcus* ecotypes. Nature **393**: 464–467. doi:10.1038/30965

Morel, F., and N. Price. 2003. The biogeochemical cycles of trace metals in the oceans. Science **300**: 944–947. doi:10.1126/science.1083545

Mosier, A. C., and C. A. Francis. 2011. Determining the distribution of marine and coastal ammonia-oxidizing archaea and bacteria using a quantitative approach. Methods Enzymol. **486**: 205–221. doi:10.1016/S0076-6879(11)86009-X

Munson, K. M., H. Lamborg, G. J. Swarr, and M. A. Saito. 2015. Mercury species concentrations and fluxes in the Central Tropical Pacific Ocean. Global Biogeochem. Cycles **29**: 656–676. doi:10.1002/2015gb005120

Murray, J. W., E. Johnson, and C. Garside. 1995. A U.S. JGOFS process study in the equatorial Pacific (EqPac): Introduction. Deep-Sea Res. **42**: 275–293. doi:10.1016/0967-0645(95)00044-Q

Nagata, T., H. Fukuda, R. Fukuda, and I. Koike. 2000. Bacterioplankton distribution and production in deep Pacific waters: Large-scale geographic variations and possible coupling with sinking particle fluxes. Limnol. Oceanogr. **45**: 426–435. doi:10.4319/lo.2000.45.2.0426

Newell, S. E., R. Babbin, A. Jayakumar, and B. B. Ward. 2011. Ammonia oxidation rates and nitrification in the Arabian Sea. Global Biogeochem. Cycles **25**: Gb4016. doi:10.1029/2010gb003940

Newell, S. E., S. E. Fawcett, and B. B. Ward. 2013. Depth distribution of ammonia oxidation rates and ammonia-oxidizer community composition in the Sargasso Sea. Limnol. Oceanogr. **58**: 1491–1500. doi:10.4319/Lo.2013.58.4.1491

Noble, A. E., A. Saito, K. Maiti, and C. R. Benitez-Nelson. 2008. Cobalt, manganese, and iron near the Hawaiian Islands: A potential concentrating mechanism for cobalt within a cyclonic eddy and implications for the hybrid-type trace metals. Deep-Sea Res. **55**: 1473–1490. doi:10.1016/j.dsr2.2008.02.010

Offre, P., M. Kerou, A. Spang, and C. Schleper. 2014. Variability of the transporter gene complement in ammonia-oxidizing archaea. Trends Microbiol. **22**: 665–675. doi:10.1016/j.tim.2014.07.007

Pester, M., C. Schleper, and M. Wagner. 2011. The Thaumarchaeota: An emerging view of their phylogeny and ecophysiology. Curr. Opin. Microbiol. **14**: 300–306. doi:10.1016/j.mib.2011.04.007

Price, M. N., S. Dehal, and A. P. Arkin. 2009. FastTree: Computing large minimum evolution trees with profiles instead of a distance matrix. Mol. Biol. Evol. **26**: 1641–1650. doi:10.1093/Molbev/Msp077

Price, N. M., and P. J. Harrison. 1987. Comparison of methods for the analysis of dissolved urea in seawater. Mar. Biol. **94**: 307–317. doi:10.1007/Bf00392945

Qin, W., and others. 2014. Marine ammonia-oxidizing archaeal isolates display obligate mixotrophy and wide ecotypic variation. Proc. Natl. Acad. Sci. USA **111**: 12504–12509. doi:10.1073/pnas.1324115111

Rafter, P. A., M. Sigman, C. D. Charles, J. Kaiser, and G. H. Haug. 2012. Subsurface tropical Pacific nitrogen isotopic composition of nitrate: Biogeochemical signals and their transport. Global Biogeochem. Cycles **26**. doi:10.1029/2010gb003979

Raimbault, P., and others. 1999. Carbon and nitrogen uptake and export in the equatorial Pacific at 150 degrees W: Evidence of an efficient regenerated production cycle. J. Geophys. Res. **104**: 3341–3356. doi:10.1029/1998jc900004

Reinthaler, T., H. M. Van Aken, and G. J. Herndl. 2010. Major contribution of autotrophy to microbial carbon cycling in the deep North Atlantic's interior. Deep-Sea Res. II **57**: 1572–1580. doi:10.1016/j.dsr2.2010.02.023

Rusch, D. B., and others. 2007. The Sorcerer II Global Ocean sampling expedition: Northwest Atlantic through eastern tropical Pacific. PLoS Biol. **5**: 398–431. doi:10.1371/journal.pbio.0050077

Saito, M. A., R. Mcilvin, D. M. Moran, T. J. Goepfert, G. R. Ditullio, A. F. Post, and C. H. Lamborg. 2014. Multiple nutrient stresses at intersecting Pacific Ocean biomes detected by protein biomarkers. Science **345**: 1173–1177. doi:10.1126/science.1256450

Santoro, A. E., L. Casciotti, and C. A. Francis. 2010. Activity, abundance and diversity of nitrifying archaea and bacteria in the central California Current. Environ. Microbiol. **12**: 1989–2006. doi:10.1111/j.1462-2920.2010.02205.x

Santoro, A. E., and K. L. Casciotti. 2011. Enrichment and characterization of ammonia-oxidizing archaea from the open ocean: Phylogeny, physiology, and stable isotope fractionation. ISME J. **5**: 1796–1808. doi:10.1038/ismej.2011.58

Santoro, A. E., and others. 2013. Measurements of nitrite production in and around the primary nitrite maximum in the central California Current. Biogeosciences **10**: 7395–7410. doi:10.5194/Bg-10-7395-2013

Santoro, A. E., and others. 2015. Genomic and proteomic characterization of "*Candidatus* Nitrosopelagicus brevis": An ammonia-oxidizing archaeon from the open ocean. Proc. Natl. Acad. Sci. USA **112**: 1173–1178. doi:10.1073/pnas.1416223112

Shiozaki, T., and others. 2016. Nitrification and its influence on biogeochemical cycles from the equatorial Pacific to the Arctic Ocean. ISME J. **10**: 2184–2197. doi:10.1038/ismej.2016.18

Sigman, D. M., L. Casciotti, M. Andreani, C. Barford, M. Galanter, and J. K. Bohlke. 2001. A bacterial method for the nitrogen isotopic analysis of nitrate in seawater and freshwater. Anal. Chem. **73**: 4145–4153. doi:10.1021/ac010088e

Sintes, E., K. Bergauer, D. De Corte, T. Yokokawa, and G. J. Herndl. 2013. Archaeal *amoA* gene diversity points to distinct biogeography of ammonia-oxidizing Crenarchaeota in the ocean. Environ. Microbiol. **15**: 1647–1658. doi:10.1111/j.1462-2920.2012.02801.x

Sintes, E., D. De Corte, N. Ouillon, and G. J. Herndl. 2015. Macroecological patterns of archaeal ammonia oxidizers in the Atlantic Ocean. Mol. Ecol. **24**: 4931–4942. doi:10.1111/mec.13365

Sintes, E., D. De Corte, E. Haberleitner, and G. J. Herndl. 2016. Geographic distribution of archaeal ammonia oxidizing ecotypes in the Atlantic Ocean. Front. Microbiol. **7**. doi:10.3389/fmicb.2016.00077

Smith, J. M., L. Casciotti, F. P. Chavez, and C. A. Francis. 2014. Differential contributions of archaeal ammonia oxidizer ecotypes to nitrification in coastal surface waters. ISME J. **8**: 1704–1714. doi:10.1038/Ismej.2014.11

Smith, J. M., J. Damasheck, F. P. Chavez, and C. A. Francis. 2015. Factors influencing nitrification rates and the abundance and transcriptional activity of ammonia-oxidizing microorganisms in the dark northeast Pacific Ocean. Limnol. Oceanogr. **61**: 596–609. doi:10.1002/lno.10235

Swan, B. K., and others. 2014. Genomic and metabolic diversity of Marine Group I Thaumarchaeota in the mesopelagic of two subtropical gyres. PLoS One **9**: e95380. doi:10.1371/journal.pone.0095380

Taylor, B. W., F. Keep, R. O. Hall, B. J. Koch, L. M. Tronstad, A. S. Flecker, and A. J. Ulseth. 2007. Improving the fluorometric ammonium method: Matrix effects, background fluorescence, and standard additions. J. North Am. Benthol. Soc. **26**: 167–177. doi:10.1899/0887-3593(2007)26[167:Itfamm]2.0.Co;2

Tolar, B. B., J. Wallsgrove, B. N. Popp, and J. T. Hollibaugh. 2016. Oxidation of urea-derived nitrogen by thaumarchaeota-dominated marine nitrifying communities. Environ. Microbiol. doi:10.1111/1462-2920.13457

Tully, B. J., C. Nelson, and J. F. Heidelberg. 2012. Metagenomic analysis of a complex marine planktonic thaumarchaeal community from the Gulf of Maine. Environ. Microbiol. **14**: 254–267. doi:10.1111/j.1462-2920.2011.02628.x

Walker, C. B., and others. 2010. Nitrosopumilus maritimus genome reveals unique mechanisms for nitrification and autotrophy in globally distributed marine crenarchaea. Proc. Natl. Acad. Sci. USA **107**: 8818–8823. doi:10.1073/pnas.0913533107

Ward, B. B. 2008. Nitrification in marine systems, p. 199–262. *In* D. G. Capone, D. A. Bronk, M. R. Mulholland, and E. J. Carpenter [eds.], Nitrogen in the marine environment. Elsevier.

Ward, B. B., and O. C. Zafiriou. 1988. Nitrification and nitric oxide in the oxygen minimum of the eastern tropical North Pacific. Deep-Sea Res. I **35**: 1127–1142. doi:10.1016/0198-0149(88)90005-2

Wilkerson, F. P., and R. C. Dugdale. 1992. Measurements of nitrogen productivity in the equatorial Pacific. J. Geophys. Res. **97**: 669–679. doi:10.1029/91jc01534

Wuchter, C., and others. 2006. Archaeal nitrification in the ocean. Proc. Natl. Acad. Sci. USA **103**: 12317–12322. doi: 10.1073/Pnas.0600756103

Yokokawa, T., Y. H. Yang, C. Motegi, and T. Nagata. 2013. Large-scale geographical variation in prokaryotic abundance and production in meso- and bathypelagic zones of the central Pacific and Southern Ocean. Limnol. Oceanogr. **58**: 61–73. doi:10.4319/lo.2013.58.1.0061

Zinser, E. R., I. Johnson, A. Coe, E. Karaca, D. Veneziano, and S. W. Chisholm. 2007. Influence of light and temperature on *Prochlorococcus* ecotype distributions in the Atlantic Ocean. Limnol. Oceanogr. **52**: 2205–2220. doi: 10.4319/Lo.2007.52.5.2205

Zubkov, M. V., A. Sleigh, P. H. Burkill, and R. J. G. Leakey. 2000. Picoplankton community structure on the Atlantic Meridional Transect: A comparison between seasons. Prog. Oceanogr. **45**: 369–386. doi:10.1016/S0079-6611(00)00008-2

Acknowledgments

The authors thank the captain and crew of the R/V *Kilo Moana*, particularly Vic Polidoro, for assistance at sea. Jacob Kendrick assisted with sample collection and analysis for pigment data. Molly George assisted with nitrate isotope sample preparation, Sarah Laperriere and Alexandra Welch assisted with DNA extraction, qPCR, and urea analyses, and James White assisted with metagenomic data analysis. Joe Jennings at Oregon State performed dissolved nutrient analyses. We thank Jason M. Smith for discussions and providing the WCB qPCR standard, the laboratory of Deborah Bronk for advice on urea measurement, and Patrick Rafter for helpful advice on water masses and circulation in the equatorial Pacific. This research was supported by United States National Science Foundation (NSF) awards OCE-1260006 to A.E.S., OCE-1031271 and OCE-1337780 to M.A.S. and C.H.L., and OCE-1259994 to C.L.D.; startup funds from the University of Maryland Center for Environmental Science (UMCES) to A.E.S.; and JGI Community Sequencing Project 1337 to C.L.D., A.E.S., and M.A.S.

Conflict of Interest

None declared.

Submitted 06 May 2016
Revised 05 December 2016
Accepted 03 February 2017

Associate editor: Anya Waite